Critical Role of Structural Order in Bipolar Redox-Active Molecules for Organic Redox Flow Batteries

Journal:	*Journal of Materials Chemistry A*
Manuscript ID	TA-ART-06-2021-004821.R2
Article Type:	Paper
Date Submitted by the Author:	05-Oct-2021
Complete List of Authors:	Li, Min; University of Utah, Department of Chemistry Agarwal, Garvit; Argonne National Labs, Materials Science Division Shkrob, Ilya; Argonne National Laboratory, Chemical Sciences and Engineering Vanderlinden, Ryan; University of Utah, Department of Chemistry Case, Julia; University of Utah, Department of Chemistry Prater, Matthew; University of Utah, Department of Chemistry Rhodes, Zayn; University of Utah, Department of Chemistry Surendran Assary, Rajeev; Northwestern University, ; Argonne National Labs, Materials Science Division Minteer, Shelley; University of Utah, Department of Chemistry

ARTICLE

Critical Role of Structural Order in Bipolar Redox-Active Molecules for Organic Redox Flow Batteries

Min Li,[a,d] Garvit Agarwal,[b,d] Ilya A. Shkrob,[c,d] Ryan T. VanderLinden,[a] Julia Case,[a] Matthew Prater,[a] Zayn Rhodes,[a,d] Rajeev S. Assary,[b,d] Shelley D. Minteer[a,d*]

Bipolar redox-active molecules (BRMs) have been suggested as a means to address crossover related issues in all-organic redox flow batteries (RFBs). In such species, electron donors (anolytes) and electron acceptors (catholytes) are linked by a chain, and the same chemical composition is used in both anode and cathode compartments to reduce chemical gradients and unbalanced ion transport. The resultant RFBs resemble the aqueous vanadium RFBs, but offer greater design flexibility and potentially more favorable electrochemical and physicochemical properties. Yet the complex trade-offs in these properties have been a complication. Here we developed a fundamental rubric to uncover the likely origins in the performance metrics of these BRMs that are salient for their use in RFBs. Methylene linked phenothiazine and phthalimide moieties were employed as model BRMs and variations in their properties and molecular conformations were evaluated by systematically varying the methylene linker. Our results revealed that even minimalistic changes in the linker length resulted in dramatic oscillations in the solubility and stability. Using crystallography, quantum chemistry, and molecular dynamics, we clarify that the seemingly fluctuating behavior is due to (1) the inter- and intra- molecular charge transfer between the donor and acceptor through bond or/and through space; (2) the formation of distinctive packing/clustering motifs. Both interactions are strongly dependent on the molecular conformation. As these structural factors modify the electronic structure of both electroactive functional groups and do not change monotonically, the structure-property response in BRMs is often complex. Accordingly, these behaviors need to be taken into account in developing BRMs and knowledge of these structural factors will allow the more rational design of BRMs for grid-scale energy storage.

Introduction

Redox flow batteries (RFBs) are a class of devices in which the decoupling of charge separation and charge storage enables unhindered battery scalability.[1-3] At present, all-vanadium aqueous redox-flow batteries (V-ARFBs)[4] are the most developed of such devices. The use of V^{2+}/V^{3+} and VO^{2+}/VO_2^+ as redox couples offers high solubility (> 1.5 M), facile redox kinetics, and life span exceeding 10,000 cycles.[5-6] An attractive feature of V-ARFBs is the suppressed crossover of active species through ion-exchange membranes (IEMs) that are used to separate cell compartments in the battery.[7] As vanadium is the only electroactive element in such devices, the storage capacity can be restored by mixing the electrolytes in the two chambers.[8] Such 'symmetric' composition also mitigates crossover-related contamination in each chamber. The redox chemistry of vanadium species, however, restricts

electrochemical cycling to a single electron exchange. Further limiting the performance is a relatively low operating potential (1.26 V) – imposed by the thermodynamic potential window of water, restricting the energy density to < 25 Wh/L.[9] Development of alternative RFB chemistries surpassing these limitations would be pivotal for widespread implementation of the technology.

Organic non-aqueous redox-flow batteries (O-NRFBs) have been suggested as potential replacements for V-ARFBs.[1, 10-11] Unlike the aqueous electrolytes, organic electrolytes provide a wide electrochemical window in excess of 3 V.[12] These non-aqueous solvents allow the use of a variety of redox-active organic molecules (ROMs), which brings significant advantages. First, it is possible to prepare ROMs using sustainable and low-cost materials.[13] Second, ROMs are composed of earth-abundant elements (such as C, N, O, S), thus providing a vast design space in developing desired properties.[14-18] Third, for ROMs, these properties can be rationally engineered.[3, 10, 19]

While these O-NRFBs are appealing, the crossover of active species has been a complication.[20] This is primarily due to the use of size-exclusion membranes (SEMs) in these devices. Due to the poor solvent compatibility[21] and low ionic conductivity of IEMs in non-aqueous electrolytes,[22] SEMs are used in O-NRFBs. Unfortunately, the selectivity of SEMs is often insufficient to reduce membrane crossover.[23] Further complications arise from using different chemical compositions in each of the cell

a. Department of Chemistry, University of Utah, 315 South 1400 East, Salt Lake City, UT 84112, USA.
b. Materials Science Division, Argonne National Laboratory, 9700 Cass Avenue, Argonne, IL 60439, USA.
c. Chemical Sciences and Engineering Division, Argonne National Laboratory, 9700 Cass Avenue, Argonne, IL 60439, USA.
d. Joint Center for Energy Storage Research (JCESR), USA
† Footnotes relating to the title and/or authors should appear here.
Electronic Supplementary Information (ESI) available: [details of any supplementary information available should be included here]. See DOI: 10.1039/x0xx00000x
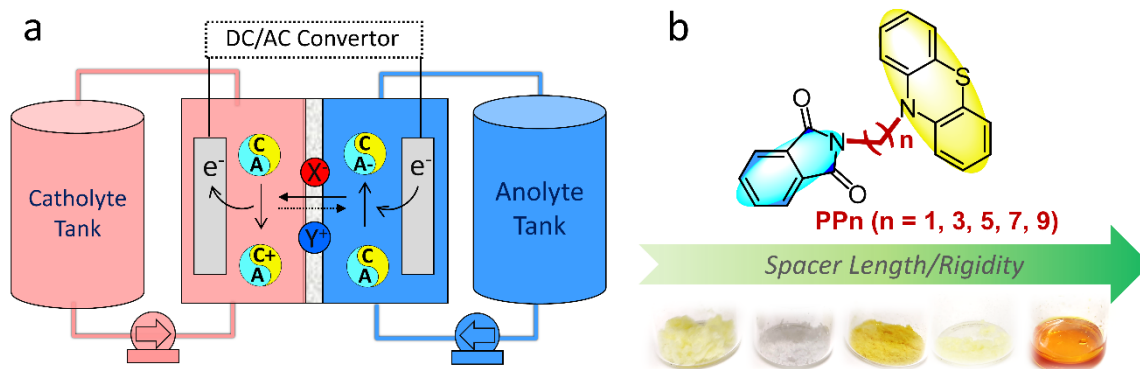
Figure 1. (a) Illustration of the working principle of symmetric redox flow cells by using bipolar redox molecules. **(b)** Chemical structures of the synthesized D-L-A molecules and photographs of the materials. Note the color of the materials that arise from charge transfer between the donor and acceptor in the molecule(s).

compartments. This 'asymmetry' and the ensuing chemical gradient facilitate undesired crossover through SEMs.[24] In recent years, redox active polymers (RAPs) were used to reduce the crossover rate, but such an approach increases the complexity of ROM chemistry[25] and slows down molecular and ionic transport.[25-29] Most importantly, RAPs in the cathode and anode compartments of a cell frequently involve two distinct active materials (called anolytes and catholytes), causing prohibitively steep concentration gradients across SEMs. Alternatively, mixed electrolytes have been used. This approach has its own problems, as it reduces power density[30-31] and introduces unbalanced mass transfer[30-32] that impedes electrochemical performance.

Bipolar redox-active molecules (BRMs) suggest a way of addressing these issues.[24] BRMs are species that include spatially separated redox moieties for positive *and* negative half-reactions.[18] In this way, it becomes possible to have the same material in both the anode and cathode compartments, in similarity to the vanadium system (Figure 1a). Since the redox active moieties are incorporated into a single molecule, the molecular and ionic species have similar transport properties in all states of charge.[33-34] Strategies in developing these BRMs have been discussed in the literature.[24, 35-36] Covalently bridging electron donors (D) and acceptors (A) using a linker (L) to create the donor-linker-acceptor (D-L-A) framework is particularly appealing due to synthetic ease and structural variability that are otherwise unattainable.[24] The donors and acceptors can be the same[37] or different,[33, 38] and the linkers provide easy targets for molecular engineering.[34, 37-38] The goal of using BRMs is to retain the benefits of vanadium system while using a flexible chemical platform with the advantages of lower cost and more favorable electrochemical properties.

While BRMs can potentially surpass mixed-ROM electrolytes, these potential advantages have not been demonstrated yet. In particular, most of the suggested BRMs (including the D-L-A systems) exhibit low cell voltage (E_{cell} <2.0 V).[34, 38-40] Another issue is the chemical stability. For instance, 1,4-diaminoanthraquinones[18] and croconate violet dianion (Croc^{2-})[41] have high theoretical capacity but poor cycling stability. While 5,10,15,20-Tetraphenylporphyrin showed stable

charging/discharging for 200 cycles, the solubility of this BRM was limited to 10 mM in dichloromethane.[15] Given such tradeoffs, recognition of systematic trends and quantitative structure-property relations would be beneficial to guide the rational design of BRMs.

Herein, we address these concerns by developing a fundamental rubric to peer into the likely origins of these complex property trade-offs. We selected D-L-A system and systematically investigated the linker (L) effect as it provides a convenient way to simulate the interactions observed between the electron donor and acceptor in BRMs. The great impact of flexible methylene chains on molecular interactions, packings[42-44] and hence on physicochemical properties of the linked molecules have been well documented. Therefore, we assessed these effects on the properties of BRMs that are critical for O-NRFB operation that include redox potentials, solubility, and cycling stability. Phenothiazine and phthalimide moieties were used as the electron donor and acceptor, respectively. The corresponding BRMs (PPn, n = 1, 3, 5, 7, 9, see Figure 1b) showed E_{cell} > 2.0 V for the first redox couple, and 2.8 V for the second redox couple (Figure S1). Our study indicates that changing the linker causes significant oscillating variation in solubility and cycling stability of these BRMs. Here we examine the scale of these variations and the causes for the observed behaviors. Our results revealed that the oscillating properties observed are a result of conformation-related interactions, highlighting the critical role of structural order in BRM systems. As these structural factors modify electronic interactions between the electron donor and acceptor, we argue that the oscillating behaviors and complex structure-property relations seen in our system are inherent to all BRMs and need to be taken into account for the rational design of BRMs.

Results and Discussions

While BRMs have been developed to suppress crossover in organic RFBs, there are complex property trade-offs in this system which impede the widespread application.[24] To understand the property trade-offs, we developed a D-L-A BRM system and systematically varied the linker to simulate plausible interactions between the

2 | J. Mater. Chem. A, 2021, **00**, 1-3

This journal is © The Royal Society of Chemistry 20xx

donor and acceptor. Here we do not seek to optimize any specific type of BRMs, but provide a fundamental case study that allows us to trace the likely origins of the complex property trade-offs observed in BRMs. Knowledge of the origins of such trade-offs will greatly facilitate the rational design of BRMs.
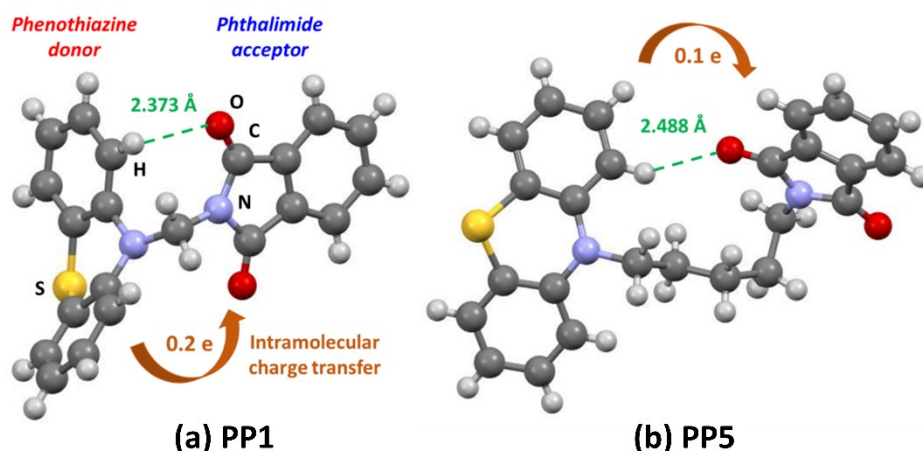

Figure 2. The structures of (a) PP1 and (b) PP5 molecules extracted from the corresponding crystals. Panel (a) shows the atom labelling. In both structures, there is a contact between a ring hydrogen in the phenothiazine donor and the carbonyl oxygen in the phthalimide acceptor. In these intramolecular CT complexes, ca. 0.2 and 0.1 electron charges are transferred from the donor to the acceptor, respectively. See the Section S3 of the Supporting Information for details.

Inter- and Intra- Molecular Interactions

For D-L-A molecules like PPn shown in Figure 1b, strong interactions between the electron donor and acceptor moieties are expected. This interaction is the *general* feature of BRMs originating from a wide gap between the redox potentials of the electron donor and acceptor in a molecule. This large difference is required to achieve high cell voltage in a symmetric cell shown in Figure 1a. The D-A interaction is already seen at the bottom of Figure 1b where it manifests itself through variation in the color of PPn compounds. The intense color arises through the occurrence of charge transfer (CT) in which a fraction of electron density is shuttled from the donor to the acceptor, so the polarized neutral molecule can be represented as $D^{\delta+}$-L-$A^{\delta-}$. The CT can be intra- and intermolecular interactions, in which intramolecular CT can occur through bond and through space, whereas intermolecular CT is through space. In the bipolar PPn molecules, both kinds of interactions are observed, with the through-bonds interaction favored in isolated molecules in dilute solutions and through-space transfer favored in the aggregated forms.

The extent of intramolecular CT depends on the proximity of the donor to the acceptor, and it reaches a maximum in an isolated PP1 molecule. In the crystal of PP1 (Figure 2a), the carbonyl oxygen atom in the phthalimide is 2.37 Å away from a hydrogen atom in the phenothiazine ring. This distance is 2.31-2.65 Å in other crystals, where the CT complex is formed between the donor and the acceptor belonging *to different* molecules. To study isolated PPn molecules in solution, density functional theory (DFT) was used. It is worth mentioning that CT is a phenomenon, rather than a quantity. The estimate of the transferred charge is only employed to map the intramolecular CT trends in isolated PPn molecules. Detail of computational methods and the estimated CT values are given in Section S3 of the Supporting Information. An extended methylene chain was assumed in most of these calculations.

According to these calculations, in the isolated PP1 molecule, ~0.2 e charge is transferred between the donor and acceptor. In the crystal of PP5, the PP5 molecule is ring-shaped, and the donor and acceptor make contact with a H…O distance of 2.49 Å, forming the intramolecular CT complex shown in Figure 2b. In this cyclical structure, through-space interactions prevail, and ~0.1 e charge is transferred from the donor to the acceptor. We expect similar polarization for CT complexes originating through random contacts of PPn molecules in solution. These interactions contribute to the clustering of these molecules affecting their solubility in electrolyte.
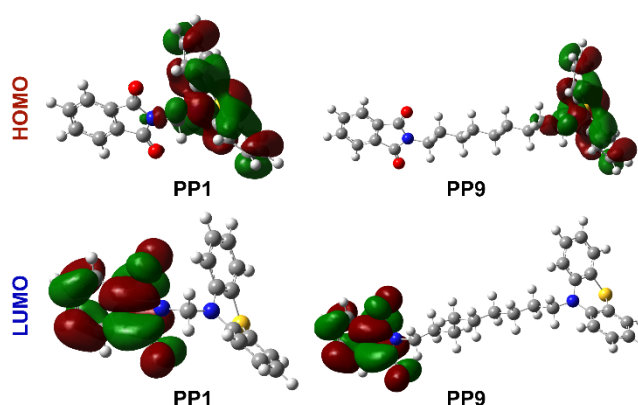

Figure 3. HOMO and LUMO isosurfaces of isolated PP1 and PP9 molecules. Details of the calculations are described in the Section S3 of the Supporting Information.
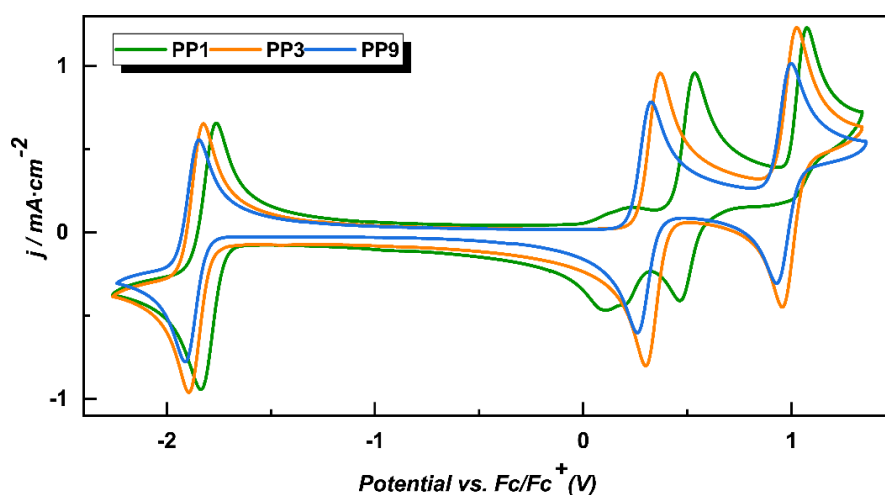
Figure 4. Cyclic voltammetry of PPn (n=1,3,9) with the traces colour coded as indicated in the plot. In these experiments, 3 mM PPn solution in 0.5 M TBAPF$_6$/MeCN were examined using a glassy carbon working electrode, a Ag/Ag$^+$ reference electrode, and a platinum counter electrode. The scan rate was 100 mV/s.

The occurrence of CT is also seen in the orbital structure of the molecules. Figure 3 shows isosurfaces for the highest occupied (HOMO) and lowest unoccupied molecular orbitals (LUMO) of neutral PP1 and PP9 molecules. The HOMO and LUMO isosurfaces of other PPn molecules are given in Table S1. As expected, the LUMO is mainly localized on the acceptor, while the HOMO is mainly localized on the donor. The spread of the wavefunction decreases as the chain becomes longer and the intramolecular CT between the terminal groups weakens, leading to more localized charge in larger molecules. In charged PPn molecules, the SOMO (Singly Occupied Molecular Orbital) and LUMO isosurfaces for the radical cation (D$^{+\bullet}$-L-A) and radical anion (D-L-A$^{-\bullet}$) states were also calculated. The spin density surfaces of radical anions were also computed (Table S2). Strong interactions between the donor and acceptor were observed in radical ions with a short methylene linker, especially for PP1. For n>3, these interactions were much weaker. This is also observed in the computed redox potentials. From PP1 to PP3, there is ~150 mV shift in the computed half potential ($E_{1/2}$) for phenothiazine oxidation, while further increasing the chain length causes relatively small variation (Table 1). These calculations indicate strong through-bond intramolecular CT in isolated PP1 molecules, a weaker CT in PP3 molecules, while for larger extended-chain molecules, intermolecular CT becomes more important. While intermolecular CT is challenging to simulate due to the complexity of molecule aggregation, both CT interactions can affect the electronic structure of each individual electroactive moieties (the donor and acceptor), which in turn, have a great impact on their stabilities. In addition, because intermolecular CT occurs through space, the formation of any nano-confinement (e.g., clustering) can significantly alter the overall CT and thus BRM properties.

	vs. Li/Li$^+$ (V)	vs. Li/Li$^+$ (V)	vs. Li/Li$^+$ (V)	vs. Li/Li$^+$ (V)
1	3.76	1.67	3.95	1.65
3	3.61	1.63	3.79	1.59
5	3.60	1.60	3.75	1.57
7	3.60	1.62	3.78	1.60
9	3.56	1.64	3.74	1.57

Cyclic Voltammetry and Transport Properties of PPn

Cyclic voltammetry (CV) of dilute PPn solutions in 0.5 M tetrabutylammonium hexafluorophosphate (TBAPF$_6$) was used to verify the predicted pattern of redox potentials in acetonitrile (MeCN). Isolated phenothiazine and phthalimide molecules undergo 2-electron charging in such solutions (Figure S1 and Section S4 of the Supporting Information), providing a potential opportunity for 2-electron BRMs. However, phthalimide dianions promptly decompose, so only 1-electron reduction of the acceptor is considered below.

In contrast, the phenothiazine donor exhibits good reversibility even in 2-electron oxidation, with an exception of PP1, for which 2-electron oxidation causes decomposition (Figure 4 and Figure S2). However, scanning through the first oxidation wave resulted in good reversibility for all PPn molecules (PP1 is shown in Figure S3), and in the following, we only examine 1-electron reactions in both moieties. In dilute solutions, only intramolecular CT is expected. In agreement with these expectations, the experimental estimates for $E_{1/2}$ showed the same trends as the ones observed in DFT calculations (Table 1), validating our molecular models.
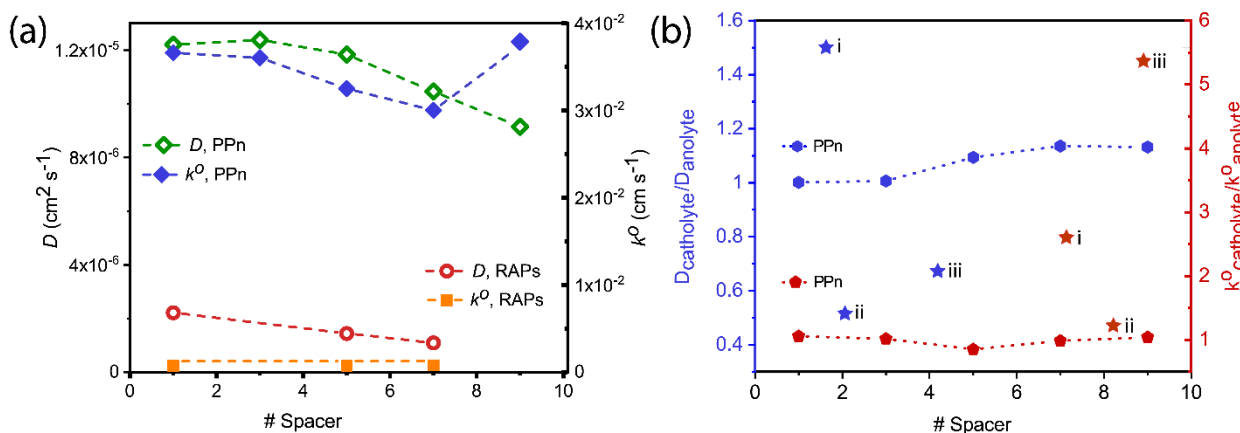
Table 1. Experimental and calculated half-wave potentials $E_{1/2}$ in acetonitrile.

PPn	Calculated		Experimental	
	$E_{1/2, ox}$	$E_{1/2, red}$	$E_{1/2, ox}$	$E_{1/2, red}$

Figure 5. (a) Diffusion coefficient and heterogeneous rate constant of the PPn radical cation and the comparison to RAPs. **(b)** The ratio of the diffusion coefficients D and rate constant k^0 for radical cation and anion of PPn. The same ratios for 1:1 mol/mol mixed electrolyte are shown for comparison. In this panel, (i-iii) refers to 1:1 mol/mol mixtures of 5,10-dihydro-5,10-dimethyl phenazine and 9-fluorenone [32]; (ii) DBMMB and 9-fluorenone,[30] and DBMMB and *N*-methylphthalimide.[31]

In addition to these redox potential data, the diffusion coefficients (D) and heterogeneous rate constants (k^o) were obtained for both redox couples. Details of applying the Randles-Sevcik equation and the Nicholson method to estimate D and k^o are given in Section S5 of the Supporting Information, and the data for acetonitrile solutions are given in Table S3 and Table S4 therein. Figure 5a show variations of D and k^o for the oxidation of the donor with the number n of atoms in the linker. These parameters are compared to the data for cyclopropenium RAPs[26] that also involve bridged structures. As suggested by this comparison, the PPn have faster diffusion and reaction rates compared to these RAPs. Additionally, for PPn, increasing the chain length does not result in significant loss of ionic mobility.

To characterize the imbalance in the kinetic properties of radical ions derived from PPn molecules, the ratios for the diffusion coefficients and rate constants of the cation and anion were used (Figure 5b). The closer these ratios are to unity, the smaller the imbalances are between the chemical fluxes in the cell. For all PPn molecules, these ratios are within 10% of unity. Because the electron donor and acceptor are covalently incorporated in one single structure, we anticipate that this balanced kinetics is a general feature for BRM systems (BRMs with extremely long flexible structures may cause deviation). To compare these data with other chemistry platforms, we examined 1:1 mol/mol 'mixed electrolytes' and found much greater imbalances in these systems (in Figure 5b, DMMB stands for 2,5-di-*tert*-butyl-1-methoxy-4-[2'-methoxyethoxy]benzene).[31] For example, for DBMMB and *N*-methylphthalimide, we obtained the ratios of 0.69 and 5.49 for $D_{catholyte}/D_{anolyte}$ and $k^o_{catholyte}/k^o_{anolyte}$, respectively. Although these ratios do not represent all the possibilities present in the mixed electrolyte system, they highlight the imbalanced kinetics exhibited in this system. Thus, *linking the catholyte and anolyte significantly reduces the imbalances related to transport and*

reactivity of charged molecules, which exemplifies the strategy of using BRMs to address such imbalances.

The electrochemical reversibility, diffusion coefficients, and rate constant of PPn were also evaluated in *N,N*-dimethylacetamide (DMA) and 1,2-dimethoxyethane (DME). DME is known to stabilize radical anions of *N*-methylphthalimide,[31] while DMA can improve PPn solubility through interactions of the phenothiazine with the amide group in the solvent molecule.[45-46] CVs of PP1 in DMA and DME solvents are shown in Figures S7 and S8, and the related parameters are summarized in Tables S5 and S6. In these two solvents, all PPn dications were unstable. Further, the higher viscosity and lower ionic conductivity of these electrolytes caused a significant decrease in the ionic diffusivity and rate constants. However, as we show below, these solvents allow for improved solubility of PPn molecules, illustrating the tradeoffs discussed in the Introduction.
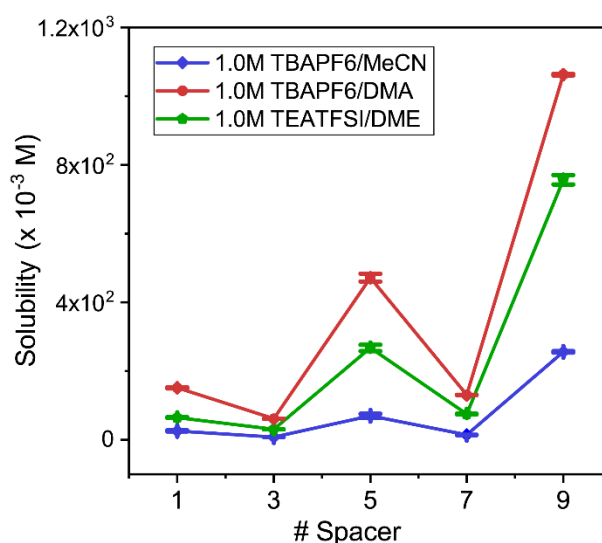

Figure 6. Solubility of PPn in different solvent systems with the color coded in the inset.

This journal is © The Royal Society of Chemistry 20xx
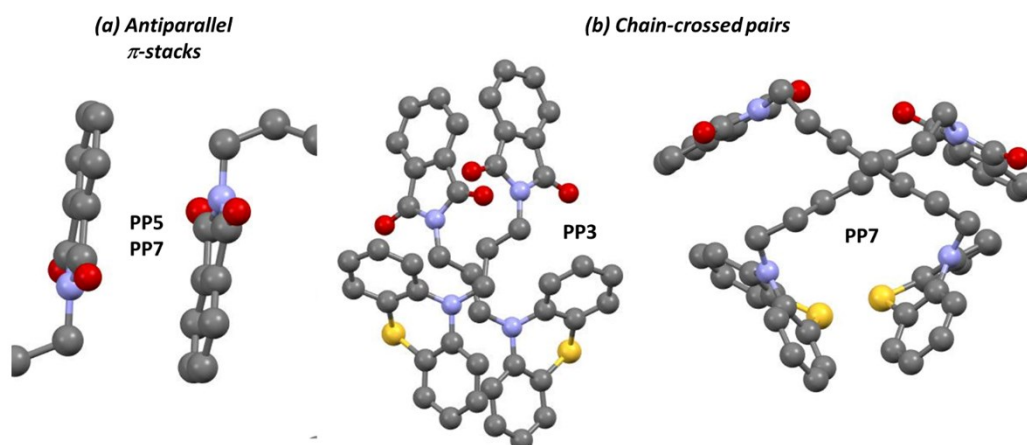
J. Mater. Chem. A., 2021, **00**, 1-3 | **5**

Figure 7. In the PPn crystals, in addition to intra- and inter- molecular CT complexes between the donor and acceptor (see Figure 2), other packing motifs include the formation of **(a)** chain-crossed pairs (observed in PP3 and PP7) and **(b)** antiparallel π--stacks between the phthalimide moieties (observed in PP5 and PP7).

Solubility trends. To achieve high power density, the solubility of BRMs needs to be high in all states of charge. To be competitive with V-ARFBs, the solubility of neutral BRMs should exceed 1 M. Many of the reported BRMs, however, have much lower solubility, even at their neutral state, which puts the BRM strategy in question.[34, 39, 47] Considering the necessity of high solubility and high ionic conductivity, we examined the solubility of the bipolar PPn molecules in 1 M electrolyte solutions in MeCN, DMA, and DME. For MeCN and DMA, the TBAPF$_6$ salt was used; for DME systems, the tetraethylammonium bistriflimide (TEATFSI) salt was used due to its greater solubility in this solvent. The experimental details are given in Section S6 of the Supporting Information (Figures S9-S12). Here we do not seek to develop highly soluble materials or screen the absolute value of the solubility at all states of charge, but to center on the neutral state and examine whether there are any variations in the solubility as a function of linkers, and whether such variations suggest mechanisms that are relevant to the complex property responses in BRMs. Further, with the factors controlling the solvation behavior of the neutral state better understood, one can consider possible approaches for solubility enhancement and other states of charge.

Figure 6 shows the solubility trends of PPn molecules. Our measurements indicate that the solvent is the main factor in defining PPn solubility in an electrolyte. For example, PP5 solubility increases 7-fold from 70 ± 6 mM in 1 M TBAPF$_6$/MeCN to 472 ± 11 mM in 1 M TBAPF$_6$/DMA. An equally large increase was observed for DME, especially for higher numbers of carbon atoms n. This indicates increasing solvent-solute interactions between the amide and ether oxygens with the phenothiazine groups.[45] Less expected was the curious oscillatory dependence of solubility on the chain length n, which was observed in all three solvents (Figure 6). The effect of electrolyte on the solubility was weak (Figure S12), suggesting that the pattern originates through *solute-solute* interactions.

Crystal structures

Since, in all cases, the solubility is limited by crystallization of BRMs from electrolyte solutions, single crystal X-ray diffraction was used to obtain structural insight into molecular packing. The unit cell parameters are given in Table S7 in Section S7 of the Supporting Information. The unit cells contain four or eight PPn molecules, with the molecular volume increasing from 410 Å^3 for PP1 to 608 Å^3 for PP9. In all crystals but PP9, CT interactions of the type shown in Figure 2 are seen, with the carbonyl oxygen atom of the phthalimide making contact with a "soft" hydrogen atom in the phenothiazine ring. In addition to these CT interactions, D-D interactions of non-planar phenothiazine rings and A-A interactions in antiparallel π-stacks of phthalimide rings are observed. The latter form a centrosymmetric structure in which the planar rings are separated by 3.7 Å (Figure 7a). These stacks are observed in PP5 and PP7 crystals. In PP9 crystal, head-to-toe, side-by-side centrosymmetric pairs of extended-chain PP9 molecules are observed (see Figure S13 in the Supporting Information).

Most relevant for the trends shown in Figure 6, the minima of solubility were observed for PP3 and PP7 crystals that showed a distinctive packing motif that was not observed in PP1 and PP5 crystals. In this motif, the methylene linkers cross each other, as shown in Figure 7b. We surmised that the formation of such chain-crossed pairs in solution can catalyze nucleation of solute molecules, i.e., solute aggregation, and turned to molecular dynamics (MD) modeling to verify our hypothesis. As this crossing is energetically favorable only for certain linkers, the curious pattern seen in Figure 6 becomes more understandable. It also becomes clear why this pattern is observed in all solvents and salts, as it depends primarily on the intricacies of *solute-solute* interactions.
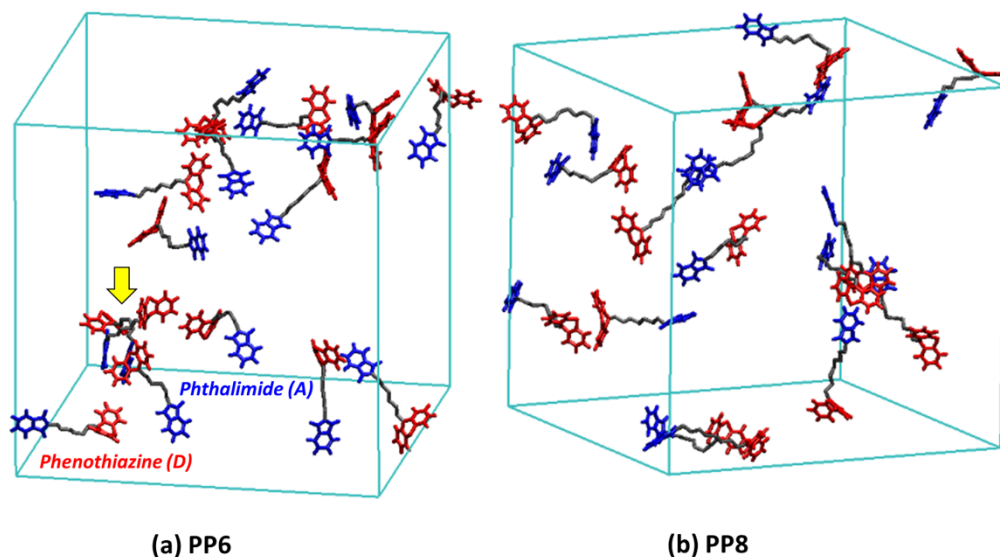
6 | J. Mater. Chem. A, 2021, **00**, 1-3

This journal is © The Royal Society of Chemistry 20xx

Figure 8. Molecular Dynamics snapshots for 0.14 M solutions of (a) PP6 and (b) PP8 in DME. The solvent molecules are not shown for clarity. The phenothiazine donor moieties are colored red, the phthalimide molecules are colored blue, and the linkers are colored gray.

Molecular Clustering in Solution

For molecular dynamics simulations, DME solution was applied as the bipolar PPn molecules are more soluble in this solvent compared to MeCN (Figure 6). The force field was derived from DFT calculations of isolated molecules as explained in Section 8 of the Supporting Information. The periodic cell conditions were performed, and 0.14 M solutions were equilibrated at 1 bar and 300 K. A sample of 200 snapshots taken over 4 ns trajectory was used to analyze clustering statistics with the assumption that this clustering reflects the observed solubility trends. In our analyses, interatomic contacts < 2.8 Å were considered as molecular proximity criterion. The model underestimates the strength of CT interactions, as no provision is made for polarization of the molecules; we are less interested in quantitative agreement than qualitative trends.

These trends became immediately obvious after a closer examination of MD snapshots. Two typical such snapshots for PP6 and PP8 solutions are shown in Figures 8a and 8b, respectively (the choice of these two systems is justified below). For the convenience of visualization, the donor moieties are colored red and the acceptor moieties are colored blue. In solution, the methylene chain is extended and the molecules interact through their terminal groups. D-A complexes of the type shown in Figure 2b, as well as A-A stacks and D-D interactions, are observed. In many aggregates, the methylene chains line along, and head-to-toe pairs are formed to maximize interactions of the terminal groups. These arrangements are seen in both panels of Figure 8, and they are similar to the pairs observed in PP9 crystals that are shown in Figure S13.

More strikingly, for some chain lengths (in this MD model, for n=6) in addition to these general modes of interaction, one observes chain-crossed pairs of the type seen in Figure 7b. Such pairs become the loci of molecular pile-up as their terminal

groups interact with the terminal groups of other PPn molecules. Figure 9a shows one such molecular pile formed around the pair indicated with the arrow in the panel. The terminal groups of this pair interact with several other PPn molecules that in turn interact with still more PPn molecules, with D-A, A-A, and D-D interactions holding the structure together. In this sense, the chain-crossed pairs seed solute aggregation and nucleation in the relatively dilute solutions. Figures 9b and 9c summarize the chain length dependence of parameters characterizing solute clusters. The inverse participation ratio (IPR), the coordination number (CN) and the spectral radius in Figure 9d are all metrics of solute clustering that increase as the average clustering increases (see the Table S8 in the Supporting Information). The minima indicated with the arrows in the plot correspond to less efficient clustering while the maxima correspond to more advanced clustering. In our model, most clustering occurs in PP4 and PP6 solutions (which can be compared to solubility minima for PP3 and PP7 in Figure 6). The clustering maxima and minima in Figure 9b correspond precisely to the systems in which chain-crossing is or is not observed in the MD snapshots, respectively, hence our choice of the two extreme systems shown in Figure 8. The same oscillatory behavior is seen in the neighbor statistics, which are the fractions of PPn molecules having exactly zero, one, or two PPn molecules contacting them. As seen from Figure 9c, the clustering maxima corresponds to the minima in the fraction of free molecules, and vice versa, and the oscillatory pattern is seen in all statistical quantities.

Thus, what appeared as a complex and "erratic" pattern seen in Figure 6, actually follows the trend observed both in crystal packing and MD simulations of solutions. Namely, for certain chains, linker-linker interactions are maximized by the crossing of these linkers, and such pairs seed BRM nucleation in

This journal is © The Royal Society of Chemistry 20xx

J. Mater. Chem. A., 2021, **00**, 1-3| **7**

solution. The resulting crystals are difficult to dissolve as the sheets of crossed fatty chains resist polar solvent. For other chain lengths, the linkers do not cross in this fashion, and such BRMs are more soluble. This linker crossing tendency cannot be traced to one specific interaction; rather it emerges in a concerted action of many such interactions. However, as we demonstrated here, using crystallography and modeling researchers can discover and potentially use these trends to improve BRM design.

A question that naturally follows from these observations is, would the chemical stability also be fluctuating, tracing the complexity of molecular interactions in the BRM systems? Before answering this question, it is worth noting that different from the solubility which is primarily determined by the presence of packing motifs that can seed nucleation, the stability of PPn molecules is also highly dependent on the intra- and intermolecular CT. Because both CT are highly sensitive to molecular conformation, we expect more complex variations in the stability of PPn molecules.

Cycling Stability Trends

In this section, we examine the cycling behavior of PPn molecules in 0.5 M TBAPF$_6$/MeCN. Capacity-controlled electrochemical cycling was performed in a symmetric, static H-cell (Figure S14 and Section S9 of the Supporting Information) with reticulated vitreous carbon electrodes in both cell compartments. A porous glass frit was used as a separator, and a reference electrode was used to control the potential of the working electrode. Both chambers of the cell initially contained 5 mM PPn solutions. This concentration is chosen to commensurate to the solubility for the least soluble PPn's shown in Figure 6. The cell was galvanostatically charged and discharged at 5 mA. The cell compartments were continuously stirred during electrolysis to homogenize the solutions. In these experiments, one can either control the oxidation potential of the donor or the reduction potential of the acceptor, as shown in Figures 10a and 10c. In this way, it is possible to characterize the cycling stability of the donor and the acceptor separately, whereas, in a full cell, capacity fade depends on the stability of both groups. As the material becomes depleted, the control potential decreases (for reduction) or increases (for oxidation); when it reaches a set cutoff value, the cycle is terminated and the direction of electric current is reversed. In this way, the loss of discharge capacity becomes related to the loss of the active material. The cutoff potential was set to 200 mV higher or lower than E$_{1/2}$ for each moiety (see below). The CVs obtained before and after cycling (Figure 10b and 10d) were used to characterize the depletion of redox-active groups and observe products of parasitic reactions. Several conclusions can be reached by examination of these cycling data.

First, we found that the donor was much more stable than the acceptor, with 94 − 99% of discharge capacity remaining after 100 cycles (Figure 10a). Coulombic efficiency (CE) remained at ~99% throughout this entire time period. In contrast, cycling of the acceptor resulted in considerable loss of discharge capacity; for PP1 and PP9 it exhibited ~17% fade after
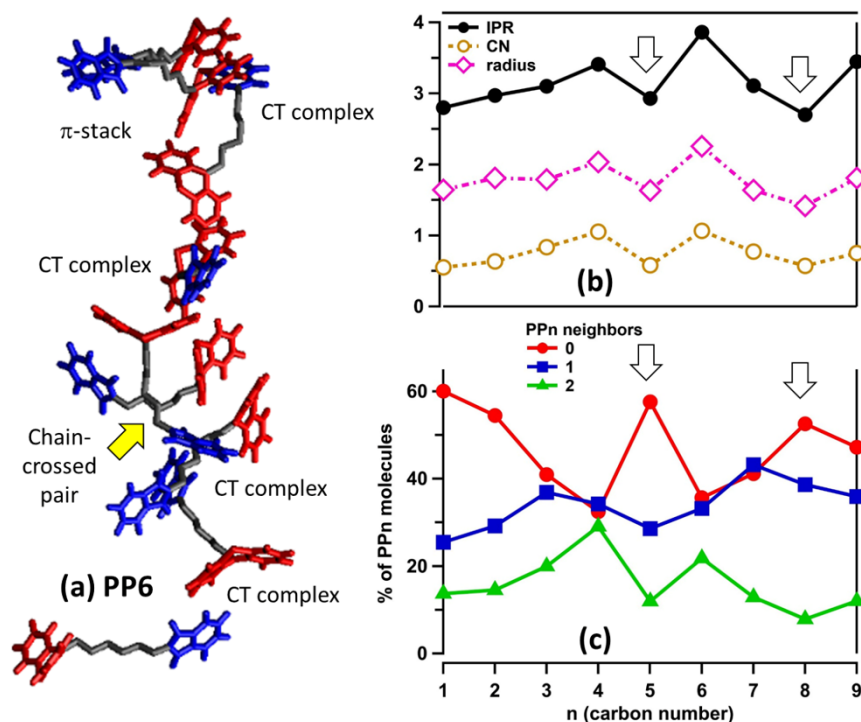

Figure 9. (a) The anatomy of a large solute cluster observed in PP6 solution in DME. The chain-crossed pair indicated with the arrow serves as a nucleation center for other PPn molecules. **(b,c)** The graphical summary of the clustering parameters (panel b) and neighbor statistics (panel c) for PPn molecules in DME (0.14 M, 300 K). See Table S8 for more information.
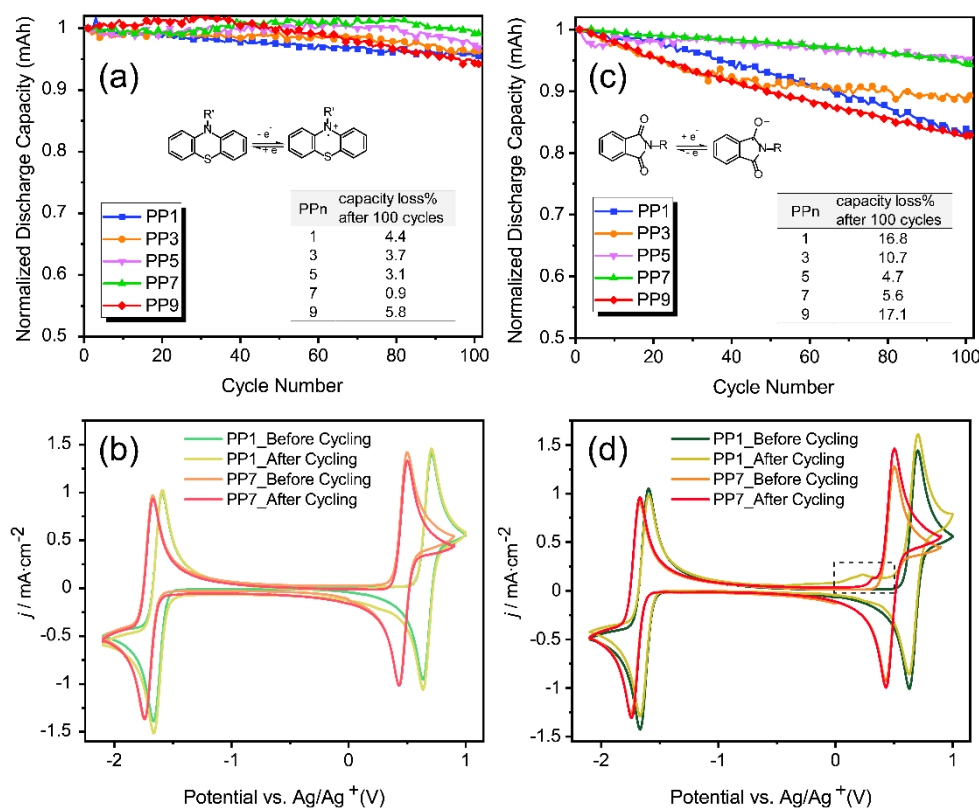
8 | J. Mater. Chem. A, 2021, **00**, 1-3

This journal is © The Royal Society of Chemistry 20xx

Figure 10. Bulk electrolysis of 5 mM PPn in 0.5 M TBAPF6/MeCN (5 mA cycling). Cycling of phthalimide acceptor (**a,b**) and phenothiazine donor (**c,d**) is shown. (**b,d**) Representative CVs for PP1 and PP7 before and after cycling of the donor and acceptor, respectively.

100 cycles (Figure 10c). Furthermore, as seen in Figure 10d, an irreversible oxidation peak appeared in the CV of the battery fluid in the working chamber after cycling of the acceptor, suggesting advanced decomposition of the phthalimide moiety. The correlation between the peak area for this wave and the capacity fade indicates that this decomposition is responsible for the capacity fade observed in the system. This poor chemical stability of the radical anion is likely due to slow reactions of this radical anion with the solvent, which were observed for isolated phthalimide molecules.[30,31] It appears that the same parasitic reaction occurs in PPn molecules involving the carbonyl group of the acceptor.

Second, there is a remarkable chain-length effect on the yield of this parasitic reaction (Figure 10c), whereas for the radical cation stability, the effect is weak (Figure 10a). From PP1 to PP7, the discharge capacity retention after 100 cycles improved from ~83% to ~95%. For *N*-methylphthalimide in the same electrolyte, the capacity fade was much faster than in these PPn molecules, reaching ~20% after 50 cycles.[31] This suggests that linking the phthalimide with the phenothiazine modulated the rates of parasitic reactions for the radical anion. This modulation can be attributed to intramolecular or intermolecular interactions involving the species.

Third, this modulation was not monotonic, with PP1 and PP9 showing rapid capacity fading that was comparable to *N*-methylphthalimide, while other PPn molecules were more resistant to decomposition. This behavior again exemplifies the complex interactions possessed in the BRM system: (i) the intramolecular CT, as aforementioned, showed the strongest for PP1, weaker for PP3, and became negligible when further extending the chain length. This through-bond CT gives rise to stability in the sequence of PP1 < PP3 ≈ PPn (n = 5,7,9). (ii) However, the unique clustering motifs formed in PPn (n = 3, 5, 7) (Figure 7) can greatly alter cycling stability. This is especially the case in dilute solutions (5 mM) where solute clustering can be significant for molecules like PP3 and PP7. In the clusters, solvent molecules are excluded from the cluster interior, which can explain slower reactions of radical anions with the solvent. Furthermore, in such clusters, there is π-stacking of phthalimide rings (also seen in the crystals) that can stabilize negative charges. Thus, while clustering is detrimental for solubility, it can improve the electrochemical stability of BRMs. For radical ions of certain unipolar ROMs, such effects have been previously observed in the literature.[48] (iii) While the intramolecular CT in PP9 is trivial, the intermolecular CT resulting from the packing of head-to-toe pair can be significant (Figure S13). The lack of chain-crossed pair further makes PP9 vulnerable to undesired interactions with the solvent. These observations align well with the surprisingly low stability of PP9. Collectively, the stability of BRMs is a result of complex environmental factors involving solvent and multiple interactions within BRMs. As such, knowledge of structural

This journal is © The Royal Society of Chemistry 20xx

J. Mater. Chem. A., 2021, **00**, 1-3 | **9**

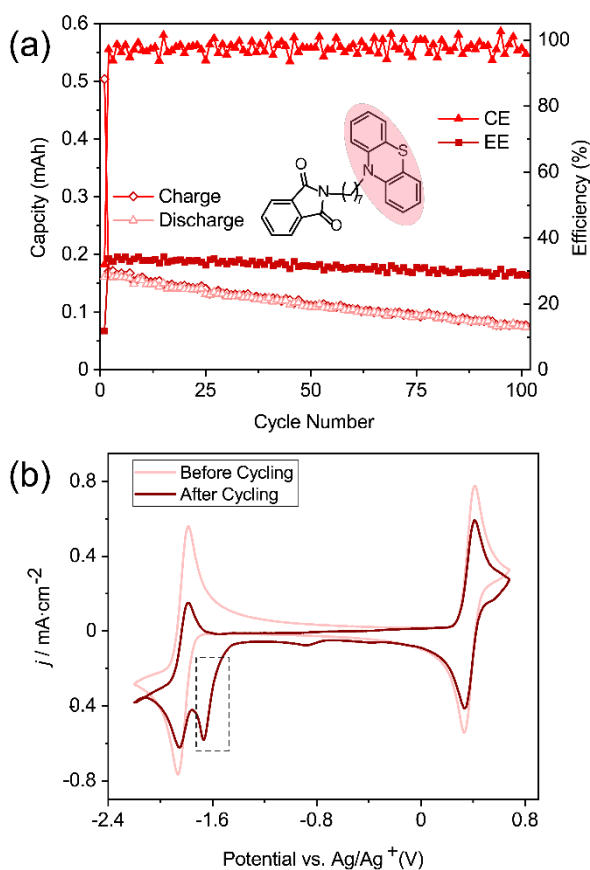factors is vital to understand and modulate BRM interactions for optimal performance.

Figure 11. Cycling stability of PP7 in TBAPF$_6$/DMA solvent system. (a) Performance in capacity, CE, and EE of cycling PP7 as catholyte for 100 cycles. (b) CV analysis before and after cycling. The phenothiazine degradation peak is indicated by the dashed square.

Fourth, in a bipolar molecule, the decomposition of one moiety compromises the stability of another moiety. Our first example of this effect is shown in Figure 10d, where it is seen that the decomposition of the acceptor results in a partial loss of redox reversibility in the donor (see the dashed square). This effect is more pronounced in TEATFSI/DME, where the acceptor decomposition is faster (Figure S15). Consequently, the intensity of the product peak in CVs for phenothiazine increased (indicated by the dashed square in Figure S15), indicating that reactions of the donor are strongly affected by the loss of the acceptor in the same bipolar molecule.

To illustrate the opposite direction of this effect, consider Figure 11a for cycling of the *donor* in DMA. As DMA is a weak base, it slowly deprotonates radical cations, so there is 54% capacity fade after 100 cycles. In contrast, isolated phthalimide molecules exhibit *greater* cycling stability in this solvent due to impeded protonation of the radical anion (Figure S16). Post-cycling analysis by CV indicated a decomposition peak near the phthalimide redox wave (see the dashed square in Figure 11b) from a species that could not be the product of phthalimide

decomposition. In this case, it is the loss of the donor that affects the redox reaction of the acceptor. These behaviors are unique for bipolar molecules.

Conclusions

While all-organic flow cells have potential advantages for achieving higher energy density at a lower cost, these advantages remain latent, as they are countered by insufficient ion selectivity and fast crossover in the separating membranes compatible with these organic electrolytes. The use of bipolar redox active molecules (BRMs) has been suggested as a strategy to address this conundrum. In many regards, such BRMs resemble the familiar vanadium system for aqueous RFBs, but offer greater design flexibility and potentially more favorable electrochemical and physicochemical properties. While the approach is tangible, it, too, has not been demonstrated to the full extent. Like unipolar redox-active molecules, BRMs show complex tradeoffs between their properties. For reasons that are not completely understood, balancing these properties proved especially difficult for BRMs. Here we address the likely causes for this behavior.

To this end, we focused on electron donor-linker-acceptor (D-L-A) molecules and changed the length of the methylene linker to simulate the donor-acceptor interactions in BRMs. Even this minimalistic change resulted in strikingly non-monotonic dependence for solubility and cycling stability, illustrating the challenges of BRMs. Crystallography, quantum chemistry, and classical molecular dynamics were used to elucidate the likely origins of such behaviors. Our conclusion is that this fluctuating response is innate to bipolar molecules, and it is likely to be their general feature.

The first peculiarity of BRMs arises from charge transfer between the donor and acceptor, which is particularly strong for high-voltage materials. This transfer can be both inter- and intra- molecular, through-bond and through-space, and it has a complex dependence on the linker and the conformation of the bipolar molecules. The energetics of this charge transfer is largely responsible for the redox energetics in the BRMs.

The second peculiarity is related to the first one. For methylene-linked BRMs, there are two modes of interaction for molecules in solution. One mode is pairing molecules with extended chains, which maximizes interactions of aromatic groups; another is chain crossing, which maximizes chain-chain and stacking interactions. A competition between these two motifs results in the characteristic "oscillatory" behavior of solution properties (including solubility) as a function of chain length.

The third peculiarity is that cycling stability for some redox moieties is strongly affected by these intra- and inter-molecular interactions. In our system, it was the stability of the radical anion that was particularly strongly affected. Non-monotonic dependence for capacity fade was observed for the phthalimide moiety, whereas no such dependence was evident for the

10 | J. Mater. Chem. A, 2021, **00**, 1-3

This journal is © The Royal Society of Chemistry 20xx

phenothiazine moiety. In this case, it is difficult to attribute this behavior to a specific interaction, but most important is the fact that such interactions (regardless of their origin) clearly matter for BRM stability.

The fourth peculiarity of bipolar molecules is that any side reaction that affects one moiety automatically affects redox reactions in another moiety, so in a full electrochemical cell, it becomes difficult to disentangle their effect on each other. Despite these complications, charge transport and redox kinetics were so well balanced for our high-voltage bipolar molecules (compared to mixed electrolytes with similar cell voltage) that it is certainly true that such systems present a great opportunity to overcome the deficiencies inherent to the use of mixed-electrolyte cells.

In summary, our study suggests why combining high solubility, electrochemical stability, and high cell voltage has been particularly difficult to achieve in bipolar molecules, and traces the challenges of these molecules identified above. With the structural and chemical factors controlling the tradeoffs between these properties better understood, a more rational approach to molecular design can be pursued. For example, crystallography and MD simulations are expected to play a critical role in defining and understanding these structural factors. Further, as flexible chains have been shown versatile in tuning the molecular geometries and thus properties,[42-44] it is anticipated that the chain-based structural functionalization (e.g., chain polarity, length, rigidity and position) will provide a versatile approach for advancing BRMs in RFB applications.

Conflicts of interest

There are no conflicts to declare.

Acknowledgements

Notes and References

1 Y. Ding, C. K. Zhang, L. Y. Zhang, Y. G. Zhou and G. H. Yu, Chem, 2019, **5**, 1964-1987.
2 Y. Ding, C. Zhang, L. Zhang, Y. Zhou and G. Yu, Chem Soc Rev, 2018, **47**, 69-103.
3 R. Chen, Curr Opin Electrochem, 2020, **21**, 40-45.
4 K. Lourenssen, J. Williams, F. Ahmadpour, R. Clemmer and S. Tasnim, J Energy Storage, 2019, **25**, 100844.
5 H. R. Jiang, J. Sun, L. Wei, M. C. Wu, W. Shyy and T. S. Zhao, Energy Storage Mater, 2020, **24**, 529-540.
6 S. Weber, J. F. Peters, M. Baumann and M. Weil, Environ Sci Technol, 2018, **52**, 10864-10873.
7 X. F. Li, H. M. Zhang, Z. S. Mai, H. Z. Zhang and I. Vankelecom, Energ Environ Sci, 2011, **4**, 1147-1160.
8 M. Ulaganathan, V. Aravindan, Q. Y. Yan, S. Madhavi, M. Skyllas-Kazacos and T. M. Lim, Adv Mater Interfaces, 2016, **3**, 1500309.
9 W. Wang, Q. T. Luo, B. Li, X. L. Wei, L. Y. Li and Z. G. Yang, Adv Funct Mater, 2013, **23**, 970-986.
10 M. Li, Z. Rhodes, J. R. Cabrera-Pardo and S. D. Minteer, Sustain Energ Fuels, 2020, **4**, 4370-4389.
11 J. Winsberg, T. Hagemann, T. Janoschka, M. D. Hager and U. S. Schubert, Angew Chem Int Ed, 2017, **56**, 686-711.
12 K. H. Hendriks, S. G. Robinson, M. N. Braten, C. S. Sevov, B. A. Helms, M. S. Sigman, S. D. Minteer and M. S. Sanford, ACS Cent Sci, 2018, **4**, 189-196.
13 B. Huskinson, M. P. Marshak, C. Suh, S. Er, M. R. Gerhardt, C. J. Galvin, X. Chen, A. Aspuru-Guzik, R. G. Gordon and M. J. Aziz, Nature, 2014, **505**, 195-198.
14 N. H. Attanayake, J. A. Kowalski, K. V. Greco, M. D. Casselman, J. D. Milshtein, S. J. Chapman, S. R. Parkin, F. R. Brushett and S. A. Odom, Chem Mater, 2019, **31**, 4353-4363.
15 T. Ma, Z. Pan, L. Miao, C. Chen, M. Han, Z. Shang and J. Chen, Angew Chem Int Ed, 2018, **57**, 3158-3162.
16 P. Geysens, Y. Li, I. Vankelecom, J. Fransaer and K. Binnemans, ACS Sus Chem Eng, 2020, **8**, 3832-3843.
17 Y. Yan, S. G. Robinson, M. S. Sigman and M. S. Sanford, J Am Chem Soc, 2019, **141**, 15301-15306.
18 R. A. Potash, J. R. McKone, S. Conte and H. D. Abruna, J Electrochem Soc, 2016, **163**, A338-A344.
19 J. A. Luo, B. Hu, M. W. Hu, Y. Zhao and T. L. Liu, Acs Energy Lett, 2019, **4**, 2220-2240.
20 S. Odom, *ACS Cent. Sci*, 2018, **4**, 140-141.
21 S. H. Shin, S. H. Yun and S. H. Moon, Rsc Adv, 2013, **3**, 9095-9116.
22 Y. Y. Lai, X. Li and Y. Zhu, Acs Appl Polym Mater, 2020, **2**, 113-128.
23 E. C. Montoto, G. Nagarjuna, J. S. Moore and J. Rodriguez-Lopez, J Electrochem Soc, 2017, 164, A1688-A1694.
24 M. Li, J. Case and S. D. Minteer, Chemelectrochem, 2021, **8**, 1-19.
25 M. Burgess, E. Chenard, K. Hernandez-Burgos, G. Nagarjuna, R. S. Assary, J. S. Hui, J. S. Moore and J. Rodriguez-Lopez, Chem Mater, 2016, **28**, 7362-7374.
26 E. C. Montoto, Y. Cao, K. Hernandez-Burgos, C. S. Sevov, M. N. Braten, B. A. Helms, J. S. Moore and J. Rodriguez-Lopez, Macromolecules, 2018, **51**, 3539-3546.
27 T. Sukegawa, I. Masuko, K. Oyaizu and H. Nishide, Macromolecules, 2014, **47**, 8611-8617.
28 J. Winsberg, T. Hagemann, S. Muench, C. Friebe, B. Haupler, T. Janoschka, S. Morgenstern, M. D. Hager and U. S. Schubert, Chem Mater, 2016, **28**, 3401-3405.

This journal is © The Royal Society of Chemistry 20xx

J. Mater. Chem. A., 2021, **00**, 1-3 | **11**

29 G. Nagarjuna, J. Hui, K. J. Cheng, T. Lichtenstein, M. Shen, J. S. Moore and J. Rodriguez-Lopez, J Am Chem Soc, 2014, **136**, 16309-16316.

30 X. Wei, W. Xu, J. Huang, L. Zhang, E. Walter, C. Lawrence, M. Vijayakumar, W. A. Henderson, T. Liu, L. Cosimbescu, B. Li, V. Sprenkle and W. Wang, Angew Chem Int Ed, 2015, **54**, 8684-8687.

31 X. L. Wei, W. T. Duan, J. H. Huang, L. Zhang, B. Li, D. Reed, W. Xu, V. Sprenkle and W. Wang, Acs Energy Lett, 2016, **1**, 705-711.

32 G. Kwon, S. Lee, J. Hwang, H. S. Shim, B. Lee, M. H. Lee, Y. Ko, S. K. Jung, K. Ku, J. Hong and K. Kang, Joule, 2018, **2**, 1771-1782.

33 Y. Z. Zhu, F. Yang, Z. H. Niu, H. X. Wu, Y. He, H. F. Zhu, J. Ye, Y. Zhao and X. H. Zhang, J Power Sources, 2019, **417**, 83-89.

34 S. Hwang, H. S. Kim, J. H. Ryu and S. M. Oh, J Power Sources, 2018, **395**, 60-65.

35 V. V. Sentyurin, O. A. Levitskiy and T. V. Magdesieva, Curr Opin Electrochem, 2020, **24**, 15-23.

36 V. V. Sentyurin, O. A. Levitskiy and T. V. Magdesieva, Curr Opin Electrochem, 2020, **24**, 6-14.

37 T. Hagemann, J. Winsberg, B. Haupler, T. Janoschka, J. J. Gruber, A. Wild and U. S. Schubert, Npg Asia Mater, 2017, **9**, e340-e340.

38 S. Hwang, H.-s. Kim, J. H. Ryu and S. M. Oh, J Power Sources, 2019, **421**, 1-5.

39 J. Friedl, M. A. Lebedeva, K. Porfyrakis, U. Stimming and T. W. Chamberlain, J Am Chem Soc, 2018, **140**, 401-405.

40 H. S. Kim, K. J. Lee, Y. K. Han, J. H. Ryu and S. M. Oh, J Power Sources, 2017, **348**, 264-269.

41 C. G. Armstrong, R. W. Hogue and K. E. Toghill, J Power Sources, 2019, **440**, 227037.

42 H. Minemawari, M. Tanaka, S. Tsuzuki, S. Inoue, T. Yamada, R. Kumai, Y. Shimoi and T. Hasegawa, Chem Mater, 2017, **29**, 1245-1254.

43 T. Lei, J.-Y. Wang and J. Pei, Chem Mater, 2013, 26, 594-603.

44 Z. Liu, G. Zhang and D. Zhang, Acc Chem Res, 2018, **51**, 1422-1432.

45 L. Zhang, Y. Qian, R. Feng, Y. Ding, X. Zu, C. Zhang, X. Guo, W. Wang and G. Yu, Nat Commun, 2020, **11**, 3843.

46 W. E. Stewart and T. H. Siddall, Chem Rev, 1970, 70, 517-551.

47 G. D. Charlton, S. M. Barbon, J. B. Gilroy and C. A. Dyker, J Energy Chem, 2019, **34**, 52-56.

48 I. A. Shkrob, T. Li, E. Sarnello, L. A. Robertson, Y. Zhao, H. Farag, Z. Yu, J. Zhang, S. R. Bheemireddy, Y. Z, R. S. Assary, R. H. Ewoldt, L. Cheng and L. Zhang, J Phys Chem B, 2020, **124**, 10226-10236.